Cement & Concrete Composites 33 (2011) 74–83

Contents lists available at ScienceDirect

Cement & Concrete Composites

journal homepage: www.elsevier.com/locate/cemconcomp

Analysis of concrete in a vertical ventilation shaft exposed to sulfate-containing groundwater for 45 years

A. Leemann *, R. Loser

Empa, Swiss Federal Laboratories for Materials Testing and Research, Überlandstr. 129, Switzerland

ARTICLE INFO

Article history:
Received 27 January 2010
Received in revised form 8 September 2010
Accepted 9 September 2010
Available online 17 September 2010

Keywords:
Concrete
Sulfate attack
Ettringite
Thaumasite
Microstructure

ABSTRACT

The concrete lining of a vertical ventilation shaft exposed to sulfate-bearing groundwater for 45 years was investigated. The concrete was characterized at several sites with different degrees of damage. Apart from strength measurements, optical and electron microscopy were the main tools used to assess the degree of damage and alteration of the concrete. The occurrence of damage appears to be related to the availability of sulfate-bearing groundwater on one side and the presence of poor-quality concrete on the other side. Most of the damage in the form of severe spalling is caused by ettringite formation. The impact of thaumasite formation with disintegration of the cement paste seems to be minor as it occurs after the concrete is already severely damaged. The mineral assemblages and the sequence of mineral formation caused by sulfate attack agree with the findings of laboratory studies and thermodynamic modeling.

1. Introduction

The interaction between concrete and sulfates in groundwater leads to a degradation of the intrinsic concrete properties. This process is commonly referred to as external sulfate attack and is a widely studied subject in cement and concrete research (e.g. [1–7]). However, the majority of the studies have been conducted on cement paste, mortar or concrete produced and exposed to sulfate in a laboratory environment. There are relatively few case studies that provide detailed information about the microstructural and chemical changes taking place in field concrete during external sulfate attack (e.g. [8–12]). Such information is essential to classify the significance of the results obtained in laboratory studies. As the main goal remains the production of sulfate-resistant concrete in real structures and not in a laboratory environment, the relation between mechanisms occurring in both has to be established.

Interaction between concrete and sulfate-containing groundwater is a common phenomenon in Swiss tunnels [11,13,14]. Sulfate-related damage with the formation of ettringite and thaumasite usually occurs in combination with leaching.

In this study, a 45 years old concrete in a vertical ventilation shaft exposed to groundwater containing sulfate was investigated. The concrete was produced using a low C_3A-cement and aggregates containing calcite. The shaft has to be accessible to control ventilation equipment installed in a recess at its bottom. Concrete deterioration led to loosening of the anchors of the elevator and severe spalling poses a constant danger during utilisation of the open elevator.

The object of this study is a detailed description of the microstructural characteristics induced on the concrete lining by sulfate attack and a clarification of the mechanisms leading to the damage. Cores of intact and damaged areas were taken. Compressive strength and total porosity were measured. Furthermore, microstructure and chemical composition were analysed using optical and electron microscopy.

2. Site description, materials and methods

2.1. Site description and materials

Three vertical shafts are used to ventilate the 3.2 km long tunnel of a motorway. Tunnel and shafts were built between 1963 and 1966. The shafts cut through sedimentary rocks and are accessible with an open elevator. One shaft shows severe deterioration of the concrete lining. It has a diameter of 6.0 m and is 72 m deep. Gypsum and anhydrite are constituents present in the surrounding sedimentary rock formations from a depth of 8 to 48 m. They alternate with limestone, dolomite and shales. The lining of ready-mixed concrete has a thickness of 15–50 cm. The variability of concrete thickness is due to the surface roughness of the rock surface. Partial spalling of the concrete surface starts at a depth of 12 m and continues down to the bottom of the shaft at 72 m. The concrete spalls parallel to its surface. The area of damaged

* Corresponding author. Tel.: +41 44 823 44 89; fax: +41 44 823 40 35.
E-mail address: andreas.leemann@empa.ch (A. Leemann).

0958-9465/$ - see front matter © 2010 Elsevier Ltd. All rights reserved.
doi:10.1016/j.cemconcomp.2010.09.012

concrete in the shaft reaches a maximum between a depth of 17 and 44 m with about 10–30% of the surface spalled (Fig. 1). There is a concentration of damage between cold joints of different concrete pours. Additionally, there are some spots with a high degree of damage often exposing the underlying rock face. The groundwater penetrates the concrete lining at these weak spots and reaches the inner surface, where it can run downwards along the concrete surface (Fig. 2; see Section 5.2).

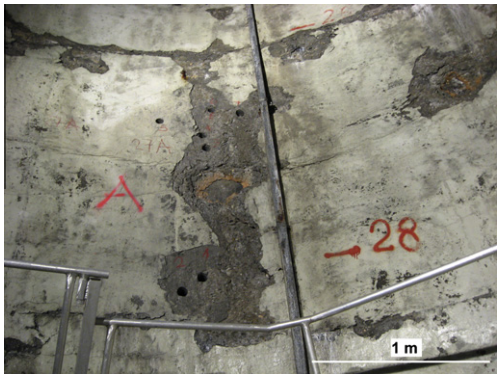

Fig. 1. Concrete with spalling at a depth of 26–29 m. At the top of the image the horizontal border between two batches of concrete can be seen. On the right-hand side of the letter "A" the rock surface is exposed.

At certain points, pipes (diameter of 20 mm) drain the water from the contact rock-concrete. The date of installation of these pipes is unknown. At the time of this investigation, the pipes were partly covered with mineral precipitations consisting of calcite and aragonite. Samples of the drained water were taken at five points and analysed.

Cores with a diameter of 50 mm of intact and severely damaged concrete were taken at three different depths (Table 1). At each depth, at least one coring site was placed in a area with severe damage and one in an area with no or little damage. The depth of the coring site is included in its name. As an example, the cores taken at site 27B are shown in Fig. 3.

The cement plant that produced the cement used for the concrete is not in operation any more. The data of the cement were obtained from the archives of the cement producer. According to these data, the cement used for concrete production was a low C_3A-type Portland cement (Table 2). According to the information in the archives, the C_3A-content was 1.9–2.1 mass%. However, a Bogue calculation with the cement composition given in Table 2 indicates no C_3A at all due to the high iron content. In any case, even if the C_3A-content is not exactly known, the cement can be regarded as a low C_3A-type. Well-rounded alluvial gravel consisting of limestone, sandstone and igneous rocks with a grain size

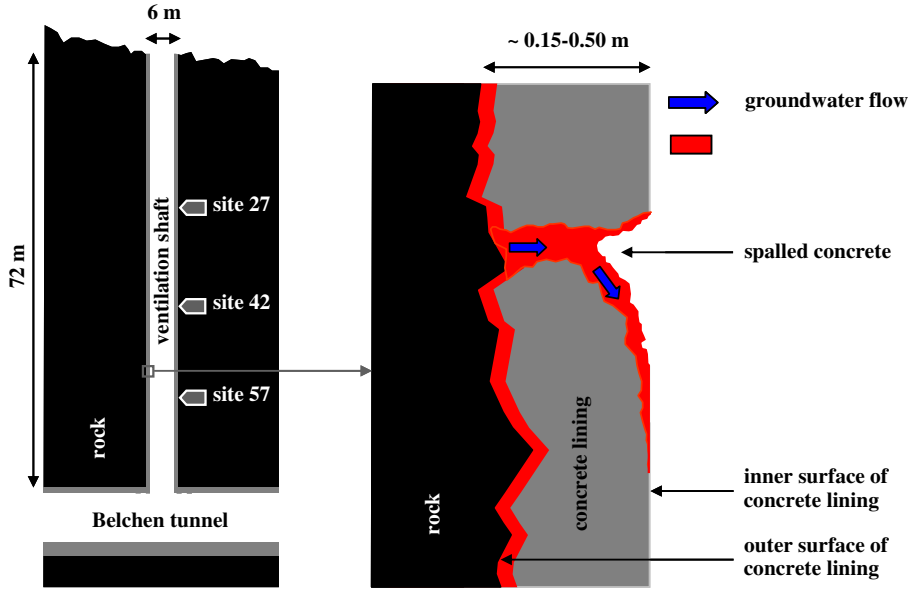

Fig. 2. Tunnel and vertical ventilation shaft with the coring sites (left); situation in the shaft with the outer surface of the concrete lining in contact with rock face/groundwater and the inner surface exposed to air.

Table 1
Coring sites.

Name	Depth (m)	Visual assessment of coring site	Number of cores	Description of cores
27A, 27B	27	Extended spalling of concrete surface	13 (l = 15–24 cm)	2–4 cracks per core perpendicular to length axis (Fig. 3), white/yellow layer (2–20 mm) at contact to rock face
27C	27	No damage visible on surface	4 (l = 20–30 cm)	0–1 cracks per core perpendicular to length axis, white/yellow layer (1–2 mm) at contact to rock face
42A	42	Locally spalled concrete surface	5 (l = 13–31 cm)	1–4 cracks per core perpendicular to length axis, white/yellow layer (2–20 mm) at contact to rock face
42B	42	No damage visible on surface	4 (l = 29–31 cm)	2–3 cracks per core perpendicular to length axis (close to rock face), white/yellow layer (1–5 mm) at contact to rock face
57A	57	Extended spalling of concrete surface	5 (l = 33–44 cm)	1–2 cracks per core perpendicular to length axis, no white/yellow layer at contact to rock face
57B	57	No damage visible on surface	5 (l = 25–49 cm)	0–1 cracks per core perpendicular to length axis, white/yellow layer (~1 mm) at contact to rock face

distribution of 0–32 mm was used as aggregates. The calcite content of the aggregates determined using thermogravimetry analysis was 7 mass%.

The concrete composition was assessed by taking into account compressive strength, pore volume and local habits of concrete production. Its cement content might have been 300–330 kg/m^3 and its water-to-cement ratio (w/c) 0.55–0.65.

2.2. Methods

The ions dissolved in the water samples were analysed with ion chromatography (IC) and pH was measured using a pH electrode.

The diameter of the cores was 50 mm. Their compressive strength was tested according to European standard EN 12504-1. Water content of saturated samples was determined by immersing five samples per core in water for 5 days. The mass difference between the end of immersion and drying at 110 °C for 2 days was used to determine the volume of the water-filled pores.

Samples for microstructural analysis were prepared from the cores. The samples were dried in an oven at 50 °C for 3 days and impregnated with epoxy resin. The impregnation of the samples enhances the strength of the cement paste allowing production of the thin sections and polishing. From each coring site, one sample was prepared for the optical microscope and one for the ESEM. For the optical microscopy (Zeiss Axioplan), thin sections (width ~50 mm, length ~95 mm, thickness ~25 μm) were prepared. For investigation with an environmental scanning electron microscope (ESEM-FEG XL30), the samples were polished, carbon coated and studied in the high vacuum mode (2.0–6.0 × 10^{-6} Torr) with an accelerating voltage of 15 kV and a beam current of 130–160 μA. The chemical composition of the concrete was determined with energy-dispersive X-ray spectroscopy (EDX). An EDAX 194 UTW detector, a Philips digital controller and Genesis Spectrum Software (Version 4.6.1) with ZAF corrections were used. The optical microscopy was used to get an overview of altered and unaltered zones, before using the ESEM for a more detailed investigation. The points analysed with EDX (100 points per analysed area or depth in the SO_3- and Ca/Si-profiles on average) were chosen randomly in a selected area of about 0.5 mm^2. An exception was the analysis used to compare the composition of inner and outer product; in this case about one half of the points were placed in each of them. "Inner product" defines the hydration products formed within the boundaries of the original cement clinker grain. The rest of the cement paste is defined as "outer product". When the electron beam meets the polished surface of the concrete sample, it interacts with a certain volume of the material. The diameter of this interaction volume is in the range of 1–3 μm with the settings described above [15]. The backscattered electrons detected by the back-scattering detector and the X-rays detected by the EDX detector are generated within this volume. As the size of specific minerals like ettringite or monosulfate is smaller than the interaction volume, the composition derived from EDX point analysis usually represents the composition of mineral assemblages and not of pure phases. However, when plots with ratios of different atoms like the Al/Ca–S/Ca-plot are used, the presence of specific minerals (in this case C–S–H, portlandite, thaumasite, ettringite, monosulfate, monocarbonate/hydrogarnet) can still be shown. As monocarbonate and hydrogarnet are both located on the Al/Ca-axis (at 0.50 and 0.68 respectively), they cannot be distinguished and only monocarbonate is shown in the plots to simplify them. When for example mainly C–S–H and some ettringite are present in the volume excited with a single point analysis, the composition in the Al/Ca–S/Ca-plot will be located between the pure phases but closer to C–S–H than ettringite. Consequently, points being located between the compositions of two pure phases indicate the presence of both. In reality, even more than two phases can be present in an analysed volume. As an example, there are points in Fig. 14 located between the line C–S–H/ettringite and thaumasite indicating the presence of these three hydrates. This approach is well established for the interpretation of point analyses of cement paste (e.g. [16–18]).

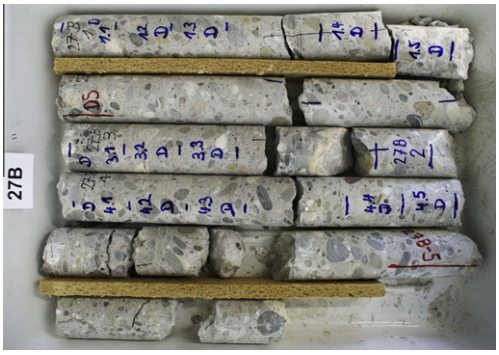

Fig. 3. Cores taken at coring site 27B. On the left side, the concrete is exposed to air. On the right is the contact to the rock face.

3. Concrete properties

In areas without visual damage of the concrete, the mean values of compressive strength vary between 42.9 and 58.0 MPa (Table 3). There is no difference in compressive strength between the outer surface of the concrete lining in contact with the rock face and

Table 2
Composition of the Portland cement (LOI = loss on ignition) and content of the main clinker phases according to Bogue calculation.

Type	CaO (%)	SiO_2 (%)	Al_2O_3 (%)	Fe_2O_3 (%)	MgO (%)	K_2O (%)	Na_2O (%)	SO_3 (%)	Insoluble (%)	LOI (%)	C_3S (%)	C_2S (%)	C_3A (%)	$C_2(A,F)$ (%)
CEM I HS	62.80	19.90	3.69	6.96	1.15	0.69	0.07	2.27	0.92	1.56	57.8	13.5	0.0	19.6

Table 3
Compressive strength and water content of concrete taken from sites without visual damage on the surface (out = surface in contact with rock, in = inner surface). "Mean in/out" is the average of three cores.

Site (m)	27C		42B		57B	
Location	Out	In	Out	In	Out	In
Compressive strength (MPa)						
Mean out/in	49.8 ± 7.8	49.0 ± 6.5	56.1 ± 3.6	58.0 ± 2.7	47.2 ± 7.3	42.9 ± 4.4
Mean core	49.4		57.1		45.1	
Water content of saturated samples (vol.%)						
Mean core	13.2		15.9		15.9	

Table 4
Compressive strength of concrete taken from sites with visual damage on surface. "Mean in/out" is the average of 2–4 cores.

Site (m)	27A		27B		42A		57A	
Core	Out	In	Out	In	Out	In	Out	In
Compressive strength (MPa)								
Mean out/in	–	40.0 ± 5.9	43.8 ± 9.8	39.4 ± 4.3	47.5 ± 2.3	51.4 ± 4.7	43.7 ± 13.1	50.0 ± 7.8
Mean core	40.0		41.6		49.5		46.9	

the inner surface of the concrete lining exposed to air and penetrating groundwater. The water content of the concrete from coring site 27C is slightly lower compared to the one from the coring sites 42B and 57B.

In areas with visual damage of the concrete, the mean values of compressive strength vary between 39.4 and 51.4 MPa (Table 4). There is no systematic change of compressive strength with depth. However, some sections could not be tested as they were damaged by cracks or the concrete fell apart during sample preparation. Especially, the white/yellow layer along the rock face was so soft that it could be easily taken apart by hand.

The differences in strength between the coring sites with damage at the inner surface and coring sites without such damage is relatively small, showing a difference of only 6 MPa. There are two explanations for this finding. Firstly, some samples of the sites with damage could not be tested due to cracks. Secondly, the damage is limited to a relatively small area along the rock face and the inner surface of the concrete lining. Generally, the standard deviation in the areas with visual damage is slightly higher than in the areas without visual damage.

4. Water analysis

The average sulfate concentration is about 2000 mg/l with a maximum at a depth of 48 m with 4230 mg/l (Table 5). The dominating cation in the groundwater is calcium with minor amounts of potassium and sodium. In a mineral water, which is bottled in a nearby spring, similar sulfate and somewhat higher calcium concentrations have been reported. Also, significant magnesium concentrations have been measured for the mineral water.

While the composition of the water interacting with the concrete can be determined, there is no information about water flow. It can be expected that water flow varies depending on the meteorological conditions.

The sulfate content of the groundwater with values up to 4 g/l is substantial. However, the concentration is far lower than that in typical accelerated laboratory tests, where concentrations of 30–50 g/l are used (e.g. [19–21]). In the water samples collected, magnesium was not measured. As dolostone is present in the rocks around the shaft, the groundwater has to contain some magnesium. Consequently, it is likely that the concrete is exposed to a combined sodium/magnesium sulfate attack.

5. Sulfate ingress

5.1. Contact between concrete lining and rock face

5.1.1. Optical microscopy

At a distance larger than 40 mm from the rock face, no alterations of the cement paste are visible. Ettringite is occasionally observed in small amounts in air voids, sometimes together with portlandite. Approaching the rock face, a few air voids are filled with thaumasite. Sometimes, a depletion of portlandite and calcium carbonate in the cement paste directly surrounding such an air void is observed (Fig. 4). With decreasing distance to the rock face, the paste starts to be altered to thaumasite. The thaumasite forms veins containing residual clinker running parallel to the rock face. The paste between the veins not altered to thaumasite contains no portlandite detectable with the optical microscope. Thaumasite is the dominating mineral in the paste at a distance to the rock face of 2 mm (57B)–25 mm (27B). Often nearly the entire paste is transformed to thaumasite (Fig. 5). At all coring sites except 57A, this severely altered zone is present. It corresponds to the white/yellow layer already identified visually (Table 1). No cracks are present in the altered zone.

5.1.2. Esem

A sample of coring site 27B was chosen to investigate the composition of the cement paste in detail. EDX analysis was performed in steps of 7 mm starting at a distance to the rock face of 72 mm.

When the rock face is approached, the SO_3-content stays below 4 mass% from a depth of 72–44 mm (Fig. 6). This value is about 1.5 mass% higher than the original SO_3-content of the cement (Table 2). Apart from C–S–H and portlandite, both ettringite and monosulfate are present. Approaching the rock face, SO_3-content increases and reaches a value of about 13 mass% at a depth of 23 mm. Most of the analysed points show the composition of C–S–H with the presence of portlandite, ettringite and monosulfate. At the depth of 23 mm, the first alterations of cement paste to thaumasite occur (Figs. 7 and 8). The mineral forms predominately along the interface between aggregates and cement paste. Thaum-

Table 5
Composition of groundwater collected in the shaft and composition of the "Eptinger" mineral water from a nearby spring (n.a. = not analysed).

Depth (m)	pH (–)	Calcium (mg Ca/l)	Magnesium (mg Mg/l)	Potassium (mg K/l)	Sodium (mg Na/l)	Sulfate (mg SO_4^{2-}/l)
12	11.7	180	n.a.	34	6	802
19	7.4	242	n.a.	55	22	1680
31	7.7	228	n.a.	11	24	1930
34	7.3	227	n.a.	5	13	1730
48	8.9	146	n.a.	86	736	4230
"Eptinger"	–	510	117	n.a.	4	1445

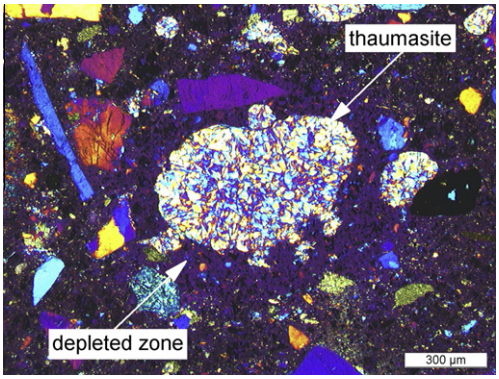

Fig. 4. Core 42A-IV (distance to rock face: 30 mm). Air void filled with thaumasite surrounded by cement paste (layer of 200–300 µm) depleted in portlandite and calcium carbonate. The irregular boundaries of the void indicate first transformations of cement paste into thaumasite. Image with crossed polarizer and gypsum plate.

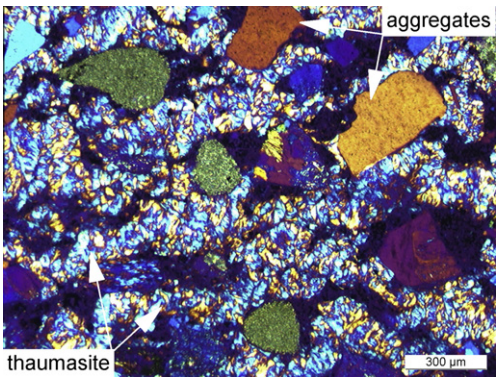

Fig. 5. Core 42A-IV (distance to rock face: 18 mm). Cement paste of concrete almost entirely altered to thaumasite at the contact to the rock face. Image with crossed polarizers and gypsum plate.

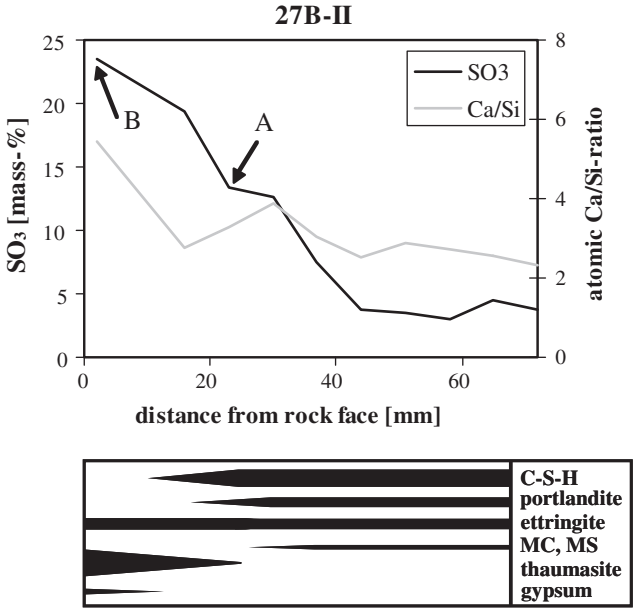

Fig. 6. Profiles of sulfate content, atomic Ca/Si-ratio and relative changes in the amount of the minerals present in the concrete in contact with the rock face. At A and B the EDX point analysis shown in Figs. 8 and 9 was conducted.

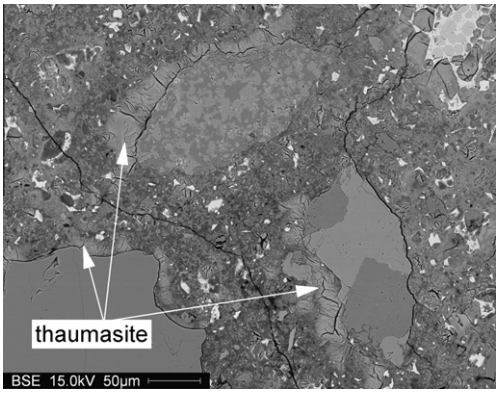

Fig. 7. Core 27B-II (distance to rock face: 23 mm). First alteration of cement paste to thaumasite. EDX point analysis conducted in this frame is shown in Fig. 8.

asite at greater depth forms only rarely in air voids. Increased magnesium concentrations can be observed occasionally along the edge of the inner product and in the inner product itself (within

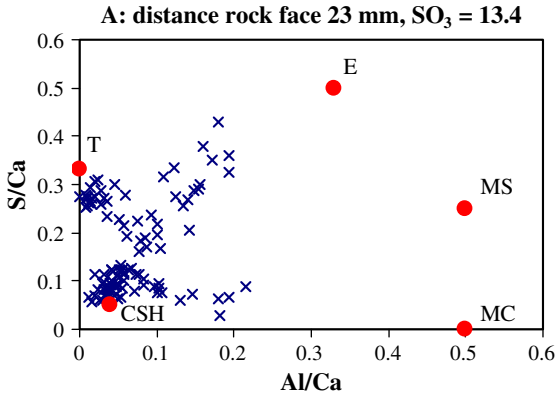

Fig. 8. Core 27B-II (distance to rock face: 23 mm). EDX point analysis of the cement paste. Average SO_3–content: 13.4 mass%. The location of the analysed area is shown in Fig. 6 (CSH = calcium–silicate–hydrate, MS = monosulfate, MC = monocarbonate, E = ettringite, T = thaumasite).

the boundaries of the former clinker grain). In the inner product, the areas of increased concentrations do not appear as small patches surrounded by C–S–H as it is typical for periclase, but the entire inner product shows an increased magnesium concentration. This phenomenon with increased magnesium level of the inner product is restricted to relatively small grains (diameter < 10 µm).

At decreasing distance to the rock face, thaumasite starts to dominate in the form of veins that are approximately parallel to the rock face. Residual clinker (C_4AF) is present in the thaumasite veins. Between the veins, there are islands not changed to thaumasite yet. In these islands, no portlandite and little C–S–H are left. The majority of the points analysed lies between the composition of C–S–H and thaumasite with some ettringite present.

The cement paste closer than 16 mm to the rock face is almost entirely altered to thaumasite (Fig. 9). Thaumasite forms needles with a length of about 2–5 µm and a width of 0.2–1.0 µm. Within this matrix, small areas (diameter of about 10 µm) with higher BSE contrast occasionally occur. They do not exhibit the needle-like habitus of thaumasite. EDX analysis shows that they consist of gypsum. As there is only a little gypsum formation, the mineral is not detected at the randomly chosen points analysed with EDX (Fig. 9). Ettringite only occurs around residual clinker, sometimes together with gypsum (see Section 5.3.1). SO_3-content of this zone ranges between 19 and 24 mass%. Ca/Si-ratio shows no significant changes with depth, ranging from 2.5 to 3.0 except very close to the rock face, where a value of 5.4 is reached.

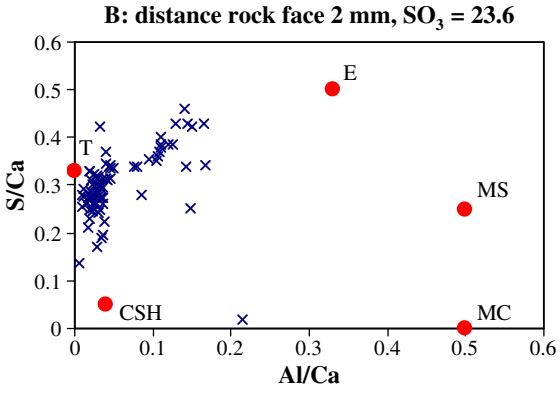

Fig. 9. Core 27B-II (distance to rock face: 2 mm). EDX point analysis of the cement paste. Average SO_3-content: 23.6 mass%. The location of the analysed area is shown in Fig. 6.

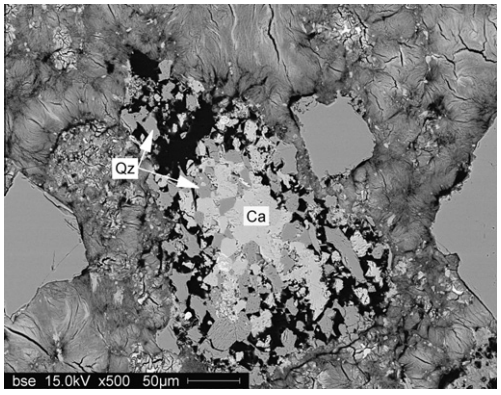

Fig. 10. Limestone containing detritic quartz embedded in a thaumasite matrix showing voids (black) caused by the dissolution of calcite (Ca = $CaCO_3$, Qz = SiO_2).

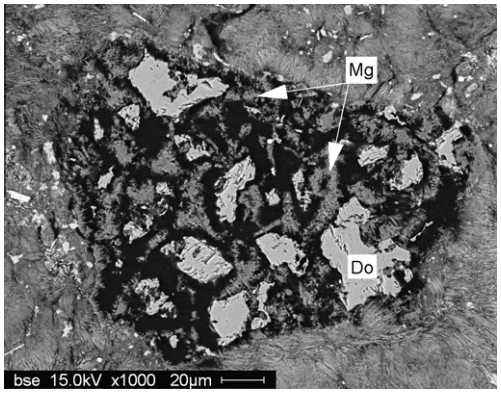

Fig. 11. Dolostone embedded in a thaumasite matrix showing voids (black) caused by the dissolution of calcium carbonate leaving a magnesium-rich residue (Do = $CaMg(CO_3)_2$).

There is no sharp transition between concrete and rock but a transition zone of several millimetres. In this transition zone, the original rock (limestone, dolomite, anhydrite, shale) is intermixed with thaumasite and gypsum. No layer with increased magnesium content occurs.

Close to the rock face, where the cement paste is completely altered to thaumasite, some aggregates show clear signs of dissolution (Fig. 10). This phenomenon is limited to aggregates containing carbonates and it does not occur in the parts with only ettringite formation. In aggregates containing calcite, the calcite is dissolved entirely leaving voids. The dissolution starts at the edges of the aggregates and proceeds inward. In the case of dolostone, the calcium carbonate is dissolved leaving a magnesium-rich product as a residue (Fig. 11).

5.1.3. Discussion

Even at the coring sites, where the concrete shows the most severe alteration along the rock face, the zone of the concrete with increased SO_3-content is relatively small and reaches only a few centimetres. Ca/Si-ratio gives no indication for severe leaching. On the one hand, the concrete in the humid environment of the shaft has to be almost saturated. Consequently, sulfate ingress has to take place mainly by diffusion and not capillary suction, which slows down the process. As an example, profiles of laboratory concrete exposed to sulfate solution (22 g/l Na_2SO_4, 5 g/l NaCl and CO_2-saturation) show a sulfate ingress by diffusion of only a few millimetres in 5 years [22]. On the other hand, it is possible that the flow of groundwater in contact with the concrete was not constant, depending on the meteorological conditions. Dry periods with no groundwater flow cannot be excluded. Although bicarbonates were not analysed, they have to be present in the groundwater, as it runs through calcite and dolomite. Their presence can significantly decrease sulfate ingress [23] and further helps to explain the relatively narrow zone with increased SO_3-content.

The amount of ettringite present in the paste, when the rock face is approached, increases with increasing sulfate content as shown by point analysis. This expansive formation of ettringite is expected to generate stress. But because the concrete along the rock face is restrained by its pipe form and the adjacent rock, no spalling can occur.

At a SO_3-concentration above 13 mass%, thaumasite is formed in the concrete along the rock face. At this concentration, the aluminium available has already reacted to ettringite. This agrees with experimental data and thermodynamic modeling [24–26] where this point was reached at a concentration of about 16 mass% using a cement with a higher C_3A-content. When air voids are not considered, the first occurrence of thaumasite generally is observed in the interfacial transition zone (ITZ) between aggregate and paste. It seems to form in areas of high porosity first. However, the residual cement clinker (mainly C_4AF) in thaumasite veins and the thaumasite matrix shows that thaumasite is not formed in cracks. The paste is rather transformed in situ to thaumasite. The difference in composition between thaumasite and C–S–H, apart from the sulphur content, is the presence of carbonate in the thaumasite and the higher calcium content of thaumasite (Ca/Si-ratio of 3.0 and 1.7 respectively). The carbonate can be derived from the groundwater, the calcite in the aggregates or both. As the rocks surrounding the shaft contain calcite and dolomite, carbonate is present in the groundwater. However, the dissolution features observed in some aggregates clearly show that they are a source for carbonate as well. Moreover, the paste surrounding an air void filled with thaumasite (Fig. 4) not only shows an absence of calcite but an absence of portlandite as well. For the formation of thaumasite, the carbonate of calcite is used and additionally the calcium of calcite, portlandite and even C–S–H [27]. Ettringite and thaumasite show a certain degree of immiscibility [28–31], as point analysis appears to confirm (Figs. 8 and 9). However, when the paste is completely altered to thaumasite, no ettringite can be identified anymore, with the exception of the inner product surrounding residual C_4AF. The stability of ettringite in a thaumasite matrix further confirms the microstructural observation in Section 5.1 that thaumasite is formed directly by a transformation of the cement paste and not through the route of ettringite formation. No hydrate in the hardened paste is stable in an environment with a sufficiently high sulphur and carbonate content. The magnesium-rich areas observed along the edge of the inner product and in the inner product of small former clinker grains are most likely caused by the presence of magnesium–silicate–hydrate and/or brucite.

As the last stage of alteration, gypsum starts to appear at a SO_3-content above 20 mass%. This again agrees with the findings in laboratory experiments and thermodynamic modeling (e.g. [24,25]). The formation of gypsum could be aided by the lack of alkali in the concrete directly at the rock face [32].

The transition zone between concrete and rock with thaumasite formation in the rock shows that not only ions move from the rock into the concrete but the reverse takes place as well.

Yearly average temperature in the shaft can be expected to be about 8–10 °C. Such a relatively low temperature has a beneficial effect on thaumasite formation (e.g. [3,25,33,34]), but the mineral can be stable up to 45 °C [7,35].

5.2. Inner surface of concrete lining

5.2.1. Optical microscopy

The variability of the microstructure at the concrete surface is relatively large. There are coring sites with neither deposits on the surface nor altered cement paste (27C, 42B, 57B). The other coring sites show the following common features approaching the inner surface of the concrete lining:

- unaltered zone,
- formation of cracks parallel to the concrete surface, mostly filled with thaumasite (Fig. 12/thickness of zone: 3–10 mm),
- calcite precipitation on the surface or formation of calcite layers in the cement paste close to the surface (thickness of zone: 1–3 mm).

5.2.2. Esem

A sample of coring site 27A was chosen to investigate the cement paste in detail. Moving from the core of the concrete lining towards its inner surface, a distance between areas investigated with EDX point analysis of several millimetres was chosen. The distance was decreased from 1 mm in a depth of 7–13 mm–0.5 mm in a depth of 0–7 mm.

SO_3-concentrations are at a level of about 5 mass% up to a depth of 12 mm (Fig. 13). Here C–S–H is the main hydrate with portlandite, ettringite, monosulfate and possibly monocarbonate. Then, SO_3-concentration increases to 8 mass% and cracks running parallel to the inner surface of the lining start to occur. Compared to the paste at lower sulfate concentration, the points indicating ettringite are more numerous. The cracks are filled with thaumasite (compare with Fig. 12). At a depth of 2–10 mm, both ettringite and thaumasite are present with possibly some monocarbonate and monosulfate (Fig. 14). The maximum SO_3-content of 17 mass% is reached at 3.7 mm. Approaching the concrete surface, the sulfate content is decreasing rapidly. In a 2 mm thick zone at the surface, layers of calcite and C–S–H depleted in Ca are alternating, leading to large fluctuations in the Ca/Si-profile (Fig. 13). At greater depths the Ca/Si-ratio is between 2.5 and 3.5. The SO_3-content is very low in these outermost layers.

At the coring sites 27A, 27B, 42A and 57A the concrete spalls parallel to its surface. One such piece of concrete from coring site 42A that was easily removed by hand was used to analyse microstructure and composition. It is plate-like with a length of about 8 cm and a width of 3 cm.

While there are only a few cracks in the inner part of the sample, extensive cracking is present towards its edges (Fig. 15). The cracks are filled with thaumasite (Fig. 16). However, in the paste only a few points indicate the occurrence of thaumasite. The

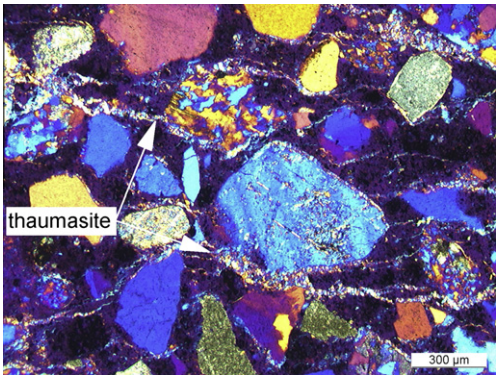

Fig. 12. Core 27A-III (distance to inner concrete surface: 10 mm). Concrete with formation of cracks filled with thaumasite running parallel to its surface. Image with crossed polarizer and gypsum plate.

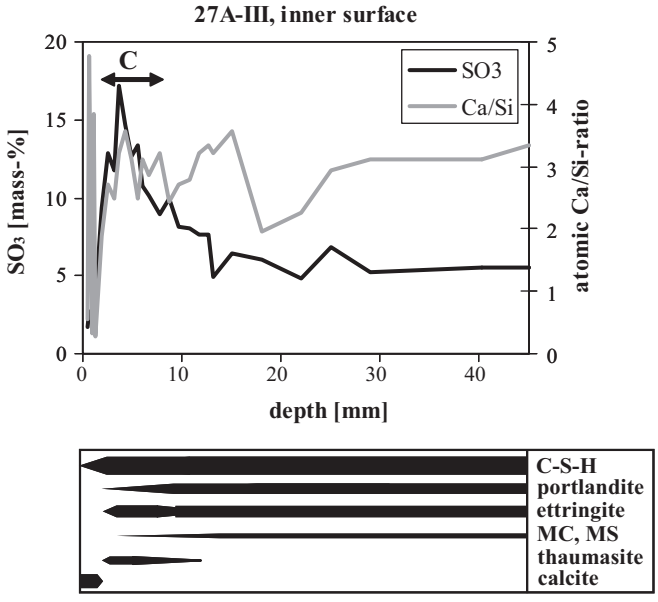

Fig. 13. Profiles of sulfate content, atomic Ca/Si-ratio and relative changes in the amount of the minerals present in the concrete exposed to air and sulfate-bearing groundwater. At C the EDX point analysis shown in Fig. 14 was conducted.

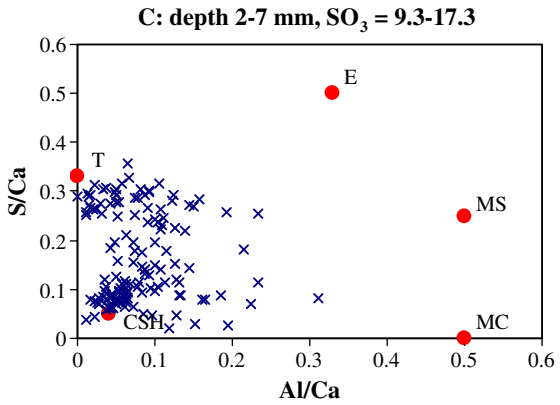

Fig. 14. Core 27A-III (distance to inner concrete surface: 2–7 mm). EDX point analysis of the cement paste. Average SO_3-content: 9.3–17.3 mass%. The location of analysed area is shown in Fig. 13.

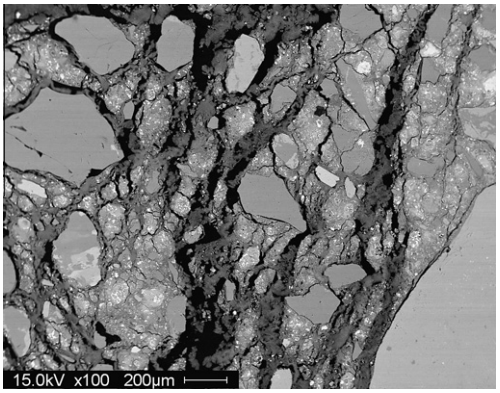

Fig. 15. Spalled concrete with extensive cracking at its edges from coring site 42A (inner surface). The cracks are filled with thaumasite.

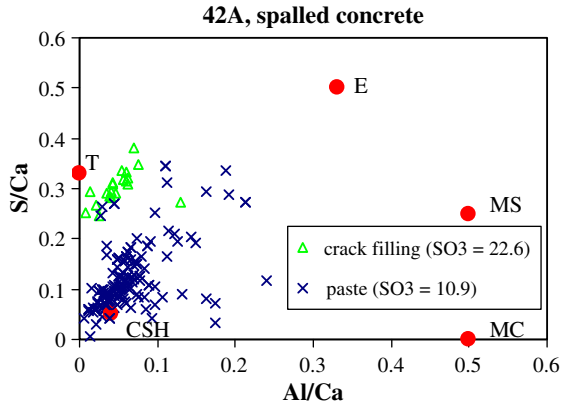

Fig. 16. EDX point analysis of crack filling and the cement paste. Average SO_3-contents are given in mass%. The location where the analysis was conducted is shown in Fig. 15.

dominating sulfate mineral is ettringite with minor amounts of monocarbonate. The main hydrate is C–S–H with some portlandite.

5.2.3. Discussion

The exposure of the concrete at the inner surface of the lining is different to the one along the rock face. Sulfate-bearing groundwater penetrates the concrete lining at specific spots (Figs. 1 and 2). These spots are either cold joints, badly compacted concrete or areas with low thickness of the concrete lining. When the groundwater reaches the inner surface, it flows downwards on the concrete surface. Sulfate ingresses the concrete either by diffusion or by capillary suction along the path of penetration. Sulfate content at the inner surface is increased only to a depth of a few centimetres similar to the concrete along the rock face. At the inner surface of the concrete lining, the amount of ettringite present increases with increasing sulfate concentration. The expansive stress caused by sulfate interaction leads to severe spalling of the concrete. Where no spalling takes place, the concrete is severely cracked. As there is no gypsum at the depth where the cracking starts, stress generation has to be attributed to ettringite formation. "Sulfate resistant" cement as used for the concrete lining causes less ettringite to form compared to Ordinary Portland cement (e.g. [36]). Additionally, the potential of C–S–H decalcification is lower because of the lower amount of ettringite formed [37]. However, it is obvious that the "sulfate resistant" cement cannot prevent severe damage and in addition offers no protection for thaumasite formation. As a consequence, the cement type seems to be of lesser importance than the w/c and with it the diffusivity and the permeability of the concrete [38,39]. Thaumasite first occurs at a SO_3-content of about 8 mass%. But in contrast to the concrete along the rock face, thaumasite forms in the cracks caused by ettringite formation. Cracks are never observed below a SO_3-concentration of about 8 mass%. This seems to be a kind of threshold for this particular concrete, where enough ettringite can form to cause sufficient expansive stress to crack the concrete. However, apart from the amount of aluminium available from calcium aluminate, the overall concrete geometry and the local degree of restraint are also important factors for depth of crack penetration and spalling [40].

Only where the highest sulfate concentrations are reached, a few local transformations of the paste into thaumasite occur. Before a wide thaumasite formation takes place, the concrete obviously spalls. Close to the concrete surface, sulfate content decreases. In this area, the high Ca/Si-ratio indicates leaching of the cement paste. The formation of the calcite layers at the concrete surface occurs when dissolved calcium from the paste reacts with the bicarbonate present in the groundwater [41–44]. The calcite formation may decrease the ingress of sulfate into the concrete [23].

In the majority of the analysed paste, the presence of monosulfate is indicated. According to thermodynamic modeling, monosulfate should not be present in systems containing calcite as it reacts to monocarbonate (e.g. [45,46]). The calcium readily available from the aggregates (calcite content of 7 mass%) and the penetrating groundwater may not have been sufficient to allow complete reaction.

The differences in the degree of damage in the shaft show that only part of the concrete lining was in contact with substantial amounts of sulfate-bearing groundwater over long periods of time. Additionally, cyclic dry and wet periods are very likely and may explain differences in degree of damage in the shaft. The chemical analysis of the groundwater indicates that the sulfate content varies in a relatively small range. As a result, the degree of damage reflects the amount of groundwater present and not the variations in sulfate concentration of the groundwater.

5.3. Composition of inner and outer product

5.3.1. Results

At a distance to the rock face of 16–30 mm, inner and outer product (see definition in Section 2.2) show differences in composition. The average SO_3-content in the inner product (19.3 mass%) is two times higher than in the outer product (Fig. 17). In the inner product two groups, one close to the composition of C–S–H and the other close to the composition of ettringite, are recognisable. In the outer product, a lower number of points head towards the composition of ettringite. In the inner and outer product, the presence of some monosulfate and monocarbonate is indicated. This composition of the paste is very similar to the one of a piece of spalled concrete from the inner surface of the lining (Fig. 18). This piece is severely cracked indicating expansive stress.

Close to the rock face, where the cement paste is almost completely altered to thaumasite, the products surrounding residual clinker have different morphology than the thaumasite matrix (Fig. 19A). EDX analysis indicates that the mineral phases present within the boundaries of the inner product are mixture of ettringite and gypsum (Fig. 19B). Analysis performed on other such grains show either a similar composition or only the presence of ettringite.

5.3.2. Discussion

In areas with increased sulfate content, the amount of sulfate in the inner and outer product is significantly different. The used ce-

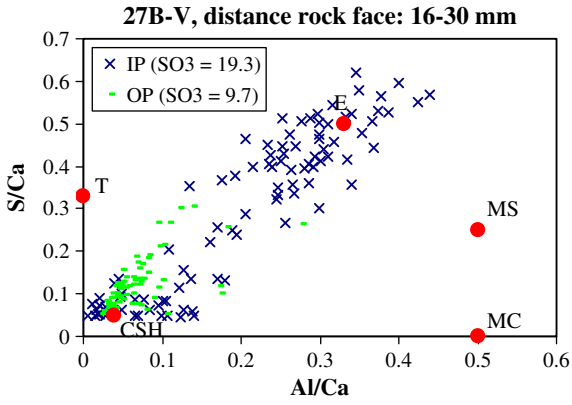

Fig. 17. Comparison between the composition of the inner and outer product in the concrete close to the rock face. The numbers in parenthesis show the average SO_3-content in mass%.

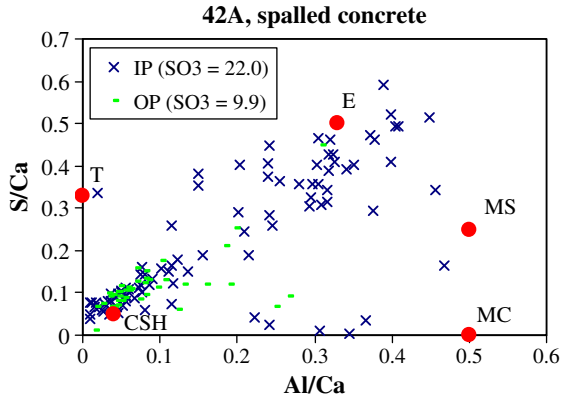

Fig. 18. Comparison between the composition of the inner and outer product in a piece of concrete spalled from the inner surface of the lining. SO_3-content is given in mass%.

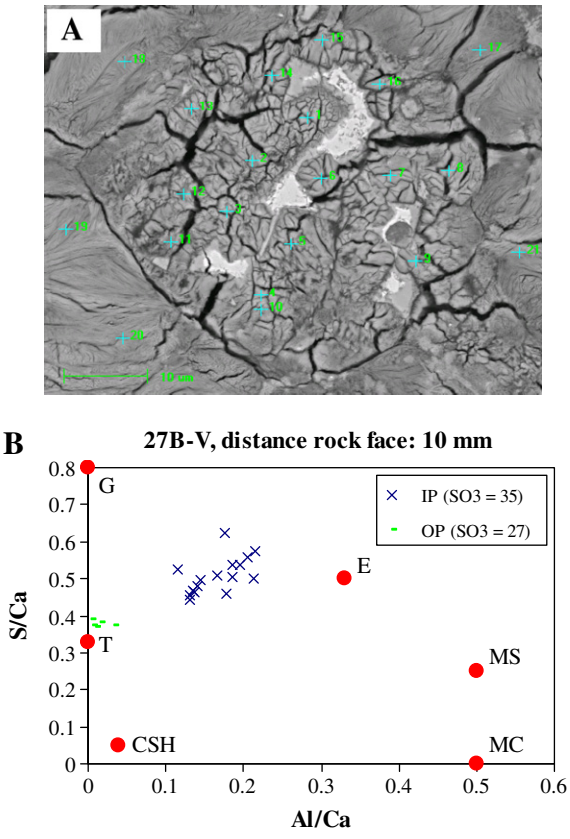

Fig. 19. Residual clinker consisting of C_4AF surrounded by inner product is embedded in a thaumasite matrix in A. B shows the composition of the points marked in A (IP = inner product (points 1–16), OP = outer product(points 17–21)). SO_3-content is given in mass%.

ment has a low C_3A-content. As a result, relatively little ettringite is formed during early hydration [47]. The aluminium in the $C_2(A,F)$ reacts relatively slowly. Due to its low mobility, most of the aluminium remains within the boundaries of the original cement grain. The ingressing sulfate reacts with the aluminium forming ettringite. The observed difference in sulfate content between inner and outer product is therefore mainly a result of the differences in aluminium content. However, this situation must have consequences for the generation of expansive stress. On the one hand, more ettringite is formed in the inner product. On the other hand, the inner product is denser than the relatively porous outer product and less pores can be filled. Even though the mechanism for stress generation is debated (e.g. [6,48–52]), it is likely that most of the expansive stress originates in the inner product. This suggestion is not directly supported by microstructural evidence as it is difficult to assess where crack formation starts. Inner and outer products exhibit microcracking in areas with increased sulfate concentrations (inner surface of the lining). In addition, some of these cracks have to be attributed to the drying needed for sample preparation.

5.4. General remarks

The concrete shows only minor leaching. The relatively static conditions are close to the conditions in laboratory test where leaching is minor as well. In general, the changes in mineralogy of the paste observed in the concrete lining show a good correlation with laboratory studies (e.g. [25,31,36,53]). The exception is the formation of gypsum that plays an important role when sulfate solutions of high concentration are used in the laboratory and is of minor importance in the studied structure. Generally, this case study provides an important validation of results obtained in laboratory tests and their interpretation.

In the majority of the other cases of sulfate attack reported in Swiss tunnels, sulfate attack goes together with severe leaching [13,14]. In such conditions, the comparability between field exposure and laboratory test is more complex and it is difficult to assess to what extent the results of the latter are applicable.

6. Conclusions

The concrete lining of a vertical ventilation shaft exposed to sulfate-bearing groundwater for 45 years was investigated.

The distribution of damages shows that the groundwater was able to penetrate the concrete and reach the inner surface of the lining only in areas of poor concrete quality or low concrete thickness. In such areas, the concrete shows severe spalling. The sulfate-resistant cement used for concrete production was not able to prevent the damages. Where no such weak areas exist, sulfate ingresses mainly by diffusion. Due to the slowness of the process, sulfate penetrated only a few centimetres at the outer surface of the concrete lining that is exposed to the rock face and the groundwater.

The main damage on the concrete lining is caused by ettringite-induced expansion leading to severe spalling at its inner surface. In this area, thaumasite is mainly formed in cracks created by the ettringite-triggered expansion. Along the rock face, no cracking or spalling occurs as the concrete is restrained. Here the cement paste is transformed in situ to thaumasite and therefore disintegrates nearly completely. Dissolution of calcite and portlandite shows that both are used as a source of carbonate and calcium respectively for thaumasite formation. Gypsum is only present in already severely deteriorated areas very close to the rock face with a SO_3-content above 20 mass%.

The inner product (hydrates within the boundaries of the former cement clinker) contains more sulfate and aluminium than the outer product, making it the most likely place where the expansive stress is generated.

The conditions in the shaft with relatively little leaching are close in this respect to the conditions in laboratory tests. Furthermore, the observed mineral assemblages and sequence of mineral formation caused by sulfate attack, ettringite–thaumasite–gypsum, corresponds to thermodynamic modeling and laboratory tests. These similarities provide an important validation of the latter.

Based on this study, a dense concrete with low *w*/*c* in a structure of homogenous quality and few weak spots (cold joints, cracks, poor compaction) seems to offer the best resistance to sulfate attack, independently of the cement and aggregates used.

Acknowledgements

The authors would like to thank J.-G. Hammerschlag for providing the data about cement composition from the archives. B. Lothenbach, W. Kunther and P. Lura are acknowledged for the critical review of the manuscript.

References

[1] Thorvaldson T. Chemical aspects of the durability of cement products. In: Proc 3rd inter symp chem cem. London, UK; 1952. p. 436–65.
[2] van Aardt JHP, Visser S. Thaumasite formation: a cause of deterioration of Portland cement and related substances in the presence of sulphates. Cem Concr Res 1975;5:225–32.
[3] Bensted J, Varma SP. A discussion of the paper Thaumasite formation: a cause of deterioration of Portland cement and related substances in the presence of sulphates by Van Aardt JHP, Visser S. Cem Concr Res 1976;6:321–2.
[4] Marchand J, Skalny J, editors. Sulfate attack mechanism. Westerville, USA: Am Ceram Soc.; 1999.
[5] Santhanam M, Cohen MD, Olek J. Mechanism of sulfate attack: a fresh look: part 1: summary of experimental results. Cem Concr Res 2002;32:915–21.
[6] Skalny J, Marchand J, Odler I, editors. Sulfate attack on concrete. London, UK: Spon Press; 2002.
[7] Macphee DE, Barnett SJ. Solution properties of solids in the ettringite – thaumasite solid solution series. Cem Concr Res 2004;34:1591–8.
[8] St John DA. An unusual case of ground water sulfate attack on concrete. Cem Concr Res 1982;12:633–9.
[9] Diamond S, Lee RJ. Microstructural alterations associated with sulfate attack in permeable concretes. American ceramic society, Inc., materials science of concrete: sulfate attack mechanisms, USA; 1999. p. 123–73.
[10] Sahu S, Badger S, Thaulow N. Evidence of thaumasite formation in Southern California concrete. Cem Concr Compos 2002;24:379–84.
[11] Romer M, Holzer L, Pfiffner M. Swiss tunnel structures: concrete damage by formation of thaumasite. Cem Concr Compos 2003;25:1111–7.
[12] Eden MA. The laboratory investigation of concrete affected by TSA in the UK. Cem Concr Compos 2003;25:847–50.
[13] Holzer L, Romer M. Corrosion of concrete: assessing the mechanisms. In: Proceedings 7th EMABM, Delft, Netherlands; 1999. p. 67–79.
[14] Pfiffner M, Holzer L. Schädigungs mechanismen der Betonkorrosion in Tunnelbauwerken. Bundesamt für Strassen, Forschungsauftrag ASTRA 1999/145, Bern; 2001.
[15] Wong HS, Buenfeld NR. Monte Carlo simulation of electron-solid interactions in cement-based materials. Cem Concr Res 2006;36:1076–82.
[16] Gollop RS, Taylor HFW. Microstructural and microanalytical studies of sulfate attack. I. Ordinary Portland cement paste. Cem Concr Res 1992;22:1027–138.
[17] Taylor HFW, Famy C, Scrivener KL. Delayed ettringite formation. Cem Concr Res 2001;31:683–93.
[18] Scrivener KL. Backscattered electron imaging of cementitious microstructures: understanding and quantification. Cem Concr Compos 2004;26:935–45.
[19] ASTM C 1012, Standard test method for length change of hydraulic-cement mortars exposed to a sulfate solution, ASTM International; 2004.
[20] SIA 262/1. Betonbau – Ergänzende Festlegungen. Schweizer Ingenieur-und Architektenverein, Zürich, Switzerland; 2003.
[21] Wittekindt W. Sulfatbeständige Zemente und ihre Prüfung. ZKG 1960;13:565–72.
[22] Tumidajski PJ, Chan GW, Philipose KE. An effective diffusivity for sulfate transport into concrete. Cem Concr Res 1995;25:1159–63.
[23] Kunther, W, Lothenbach, B, Scrivener KL. Influence of different sulphate environments on the properties of ordinary Portland cement. 17. IBAUSIL, Weimar, Germany; 2009. 6 p.
[24] Juel I, Herfort D, Gollop R, Konnerup-Madsen J, Jakobsen HJ, Skibsted J. A thermodynamic model for predicting the stability of thaumasite. Cem Concr Compos 2003;25:867–72.
[25] Schmidt T, Lothenbach B, Romer M, Scrivener K, Rentsch D, Figi R. A thermodynamic and experimental study of the conditions of thaumasite formation. Cem Concr Res 2008;38:337–49.
[26] Schmidt T, Lothenbach B, Romer M, Neuenschwander J, Scrivener KL. Physical and microstructural aspects of sulfate attack on ordinary and limestone blended Portland cements. Cem Concr Res 2009;39:1111–21.
[27] Bellmann F, Stark J. The role of calcium hydroxide in the formation of thaumasite. Cem Concr Res 2008;38:1154–61.
[28] Edge RA, Taylor HFW. Crystal structure of thaumasite, $[Ca_3Si(OH)_6 12H_2O](SO_4)(CO_3)$. Acta Cryst B 1971;27:594–601.
[29] Barnett SJ, Adam CD, Jackson ARW. Solid solutions between ettringite and thaumasite. J Mater Sci 2000;35:4109–14.
[30] Barnett SJ, Macphee DE, Crammond NJ. Extent of immiscibility in the ettringite–thaumasite system. Cem Concr Compos 2003;25:851–5.
[31] Macphee D, Diamond S. Thaumasite in cementitious materials. Cem Concr Compos 2003;25:805–7.
[32] Bellmann F, Möser B, Stark J. Influence of sulfate solution concentration on the formation of gypsum in sulfate resistance test specimen. Cem Concr Res 2006;36:358–63.
[33] Bensted J. Thaumasite – background and nature in deterioration of cements, mortars and concretes. Cem Concr Compos 1999;21:117–21.
[34] Pipilikaki P, Papageorgiou D, Teas C, Chaniotakis E, Katsioti M. The effect of temperature on thaumasite formation. Cem Concr Compos 2008;30:964–9.
[35] Glasser FP, Marchand J, Samson E. Durability of concrete – degradation phenomena involving detrimental chemical reactions. Cem Concr Res 2008;38:226–46.
[36] Gollop RS, Taylor HFW. Microstructural and microanalytical studies of sulfate attack. II. Sulfate-resisting Portland cement: ferrite composition and hydration chemistry. Cem Concr Res 1994;24:1347–58.
[37] Gollop RS, Taylor HFW. Microstructural and microanalytical studies of sulfate attack III. Sulfate resisting Portland cement: reactions with sodium and magnesium sulfate solutions. Cem Concr Res 1995;25:1581–90.
[38] Monteiro PJM, Kurtis KE. Time to failure for concrete exposed to severe sulfate attack. Cem Concr Res 2003;33:987–93.
[39] Irassar EF. Sulfate attack on cementitious materials containing limestone filler – a review. Cem Concr Res 2009;39:241–54.
[40] Lura P, Jensen OM, Weiss J. Cracking in cement paste induced by autogenous shrinkage. Mater Struct 2009;42:1089–99.
[41] Duguid A, Radonjic M, Scherer G. The effect of carbonated brine on well cement used in geologic formations. In: 12th ICCC, Montreal, Canada; 2007. TH4-10.2.
[42] Neuville N, Lecolier E, Aouad G, Daminot D. Characterisation and modelling of physico-chemical degradation of cement-based materials used in oil wells. In: Proc. RILEM CONMOD'08', Delft, Netherlands; 2008. p. 191–8.
[43] Leemann A, Lothenbach B, Hoffmann C. Biologically induced concrete deterioration in a wastewater treatment plant assessed by combining microstructural analysis with thermodynamic modeling. Cem Conc Res 2010;40:1157–64.
[44] Leemann A, Lothenbach B, Hoffmann C. Influence of water hardness on concrete surface deterioration caused by nitrifying biofilms in waste water treatment plants. Int Biodeter Biodegrad 2010;64:489–98.
[45] Matschei T, Lothenbach B, Glasser FP. The role of calcium carbonate in cement hydration. Cem Concr Res 2007;37:551–8.
[46] Lothenbach B, Le Saout G, Gallucci E, Scrivener K. Influence of limestone on the hydration of Portland cements. Cem Concr Res 2008;38:848–60.
[47] Taylor HFW. Cement chemistry. Thomas Telford Publishing, London, UK; 1997.
[48] Mehta PK. Further evidence for expansion of ettringite by water adsorption. J Am Ceram Soc 1978;61:179–81.
[49] Ogawa K, Roy DM. C_4A_3S hydration, ettringite formation, and its expansion mechanism: I. expansion; ettringite stability. Cem Concr Res 1981;11:741–50.
[50] Odler I, Colán-Subauste J. Investigations on cement expansion associated with ettringite formation. Cem Concr Res 1999;29:731–5.
[51] Clark SM, Colas B, Kunz M, Speziale S, Monteiro PJM. Effect of pressure on the crystal structure of ettringite. Cem Concr Res 2008;38:19–26.
[52] Flatt RJ, Scherer GW. Thermodynamics of crystallization stresses in DEF. Cem Concr Res 2008;38:325–36.
[53] Irassar EF, Bonavetti VL, González M. Microstructural study of sulfate attack on ordinary and limestone Portland cements at ambient temperature. Cem Concr Res 2003;3:31–41.